Electronic Supplementary Material (ESI) for Journal of Materials Chemistry A.
This journal is © The Royal Society of Chemistry 2020

Electronic supplementary information

Anion-modulated nickel-based nanoheterostructures as high performance electrocatalysts for hydrogen evolution reaction

Yang Li, Yugan Gao, Sen Yang, Chengqi Wu, and Yiwei Tan*

State Key Laboratory of Materials-Oriented Chemical Engineering, School of Chemistry and Chemical Engineering, Nanjing Tech University, Nanjing 211816, China, Email: ytan@njtech.edu.cn

Experimental section

Materials

Selenic acid (H_2SeO_4, Alfa Aesar, 40% aqueous solution), nickel(II) acetylacetonate ($Ni(acac)_2$, Alfa Aesar, 96%), n-octyl mercaptan (Alfa Aesar, 98%), 2-methoxy-5-nitroaniline (MNA, Alfa Aesar, > 98%), 1-octadecene (ODE, Alfa Aesar, 90%), oleylamine (OAm, Alfa Aesar, approximate C18-content 80-90%), tri-n-octylphosphine (TOP, Sigma-Aldrich, 90%), N-methyl-2-pyrrolidinone (NMPD, Alfa Aesar, 99%), nickel foam (1.5-mm thickness, Ailantian Advanced Technology Materials Co. Ltd.) were purchased from various commercial sources and used without any further purification if not otherwise specified. Ultrapure water (18.2 MΩ) produced with a Milli-Q purification system was used in the synthesis and electrochemical measurements.

Electrode preparation

For the preparation of Pt/C working electrode as a reference, 2 mg of Pt/C (20 wt% Pt) and 40 μL of Nafion solution (5 wt%) were dispensed in 460 mL of water/ethanol (v/v = 4 : 1) and then sonicated for 30 min to form a homogenous ink dispersion. Afterward, 200 μL of the dispersion was drop-casted on a piece of Ni foam with an exposure area of 0.5 cm^2 to obtain a loading amount of 0.16 mg cm^{-2} for the electroactive Pt.

Characterization of materials

Scanning electron microscopy (SEM) images were acquired using a Hitachi S-4800 field-emission scanning electron microscope to investigate the morphology of the catalysts, operating at an acceleration voltage of 5 kV. Transmission electron microscopy (TEM) images were obtained using an FEI Tecnai G2 Spirit Bio TWIN transmission electron microscope operated at an accelerating voltage of 100 kV. High-resolution TEM (HRTEM) and scanning TEM (STEM) micrographs, and EDX elemental maps were acquired using an FEI Tecnai G2 F20 S-TWIN transmission electron microscope operated at 200 kV to probe the crystallographic structure and composition of samples. STEM micrographs and EDX elemental maps were obtained in high-angle annular dark field (HAADF) mode to provide the bulk chemical composition of samples. The specimens for TEM observations were scratched from the NF support and sonicated before dropping them onto 300 mesh carbon-coated copper or molybdenum grids. Atomic force microscopy (AFM) measurements were implemented by Vecco Dimension 3100 SPM system. To analyze the surface composition and elemental oxidation states of samples, X-ray photoelectron spectroscopy (XPS) measurements were carried out using a Kratos Axis Supra (Kratos Analytical, Japan) spectrometer at 15 kV and 10 mA with a hemispherical energy analyzer, employing a monochromated microfocused (300 × 700 μm^2) Al-Kα (hv = 1486.58 eV) X-ray source. Samples for XPS measurements were carefully scratched from the NF support and then sputtered by repeated cycles of Ar^+ ions to obtain clean sample surfaces. The binding energies (BEs) of the core levels were calibrated by setting the adventitious C 1s peak at 284.8 eV. Survey spectra of the samples in the BE range of 0–1000 eV and the core level spectra of the elemental signals were collected with a step size of 1 and 0.1 eV, respectively. To obtain the phase and structure of samples, the X-ray diffraction (XRD) patterns were recorded using a Rigaku SmartLab diffractometer with a Cu Kα X-ray source (λ = 1.5406 Å, generated at 40 kV and 100 mA) at a scanning rate of 0.06° s^{-1}, and scanned in the

Bragg−Brentano mode from 2θ of 10° to 90° in 0.02° increments. The active materials were carefully scratched from the NF support and then used as the specimen for XRD characterization after cleaning treatment. The chemical composition of the catalyst was determined by EDX quantitative analysis and inductively coupled plasma atomic emission spectrometry (ICP-AES, Prodigy, Leeman Labs Inc., λ = 165–800 nm, As = 200 nm) measurements after dissolving the sample in aqua regia.

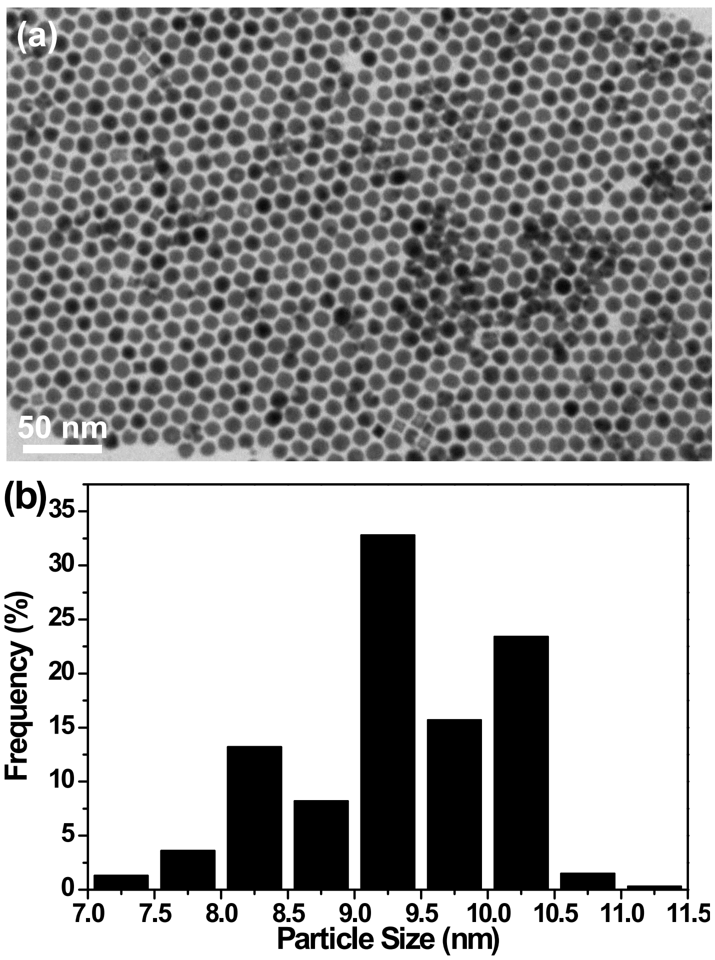

Figure S1. (a) TEM image and (b) the corresponding size distribution histogram of the as-prepared Ni_2P NPs.

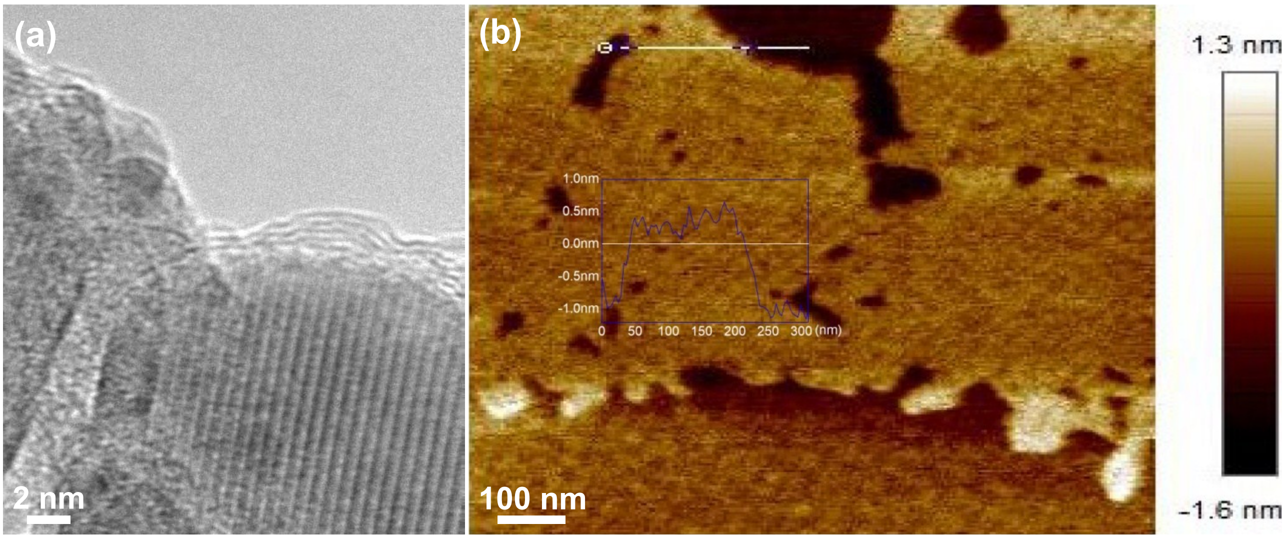

Figure S2. (a) HRTEM and (b) AFM images of Ni_3Se_4 NSs. The inset in panel (b) showing the height profiles to demonstrate the thicknesses of Ni_3Se_4 NSs.

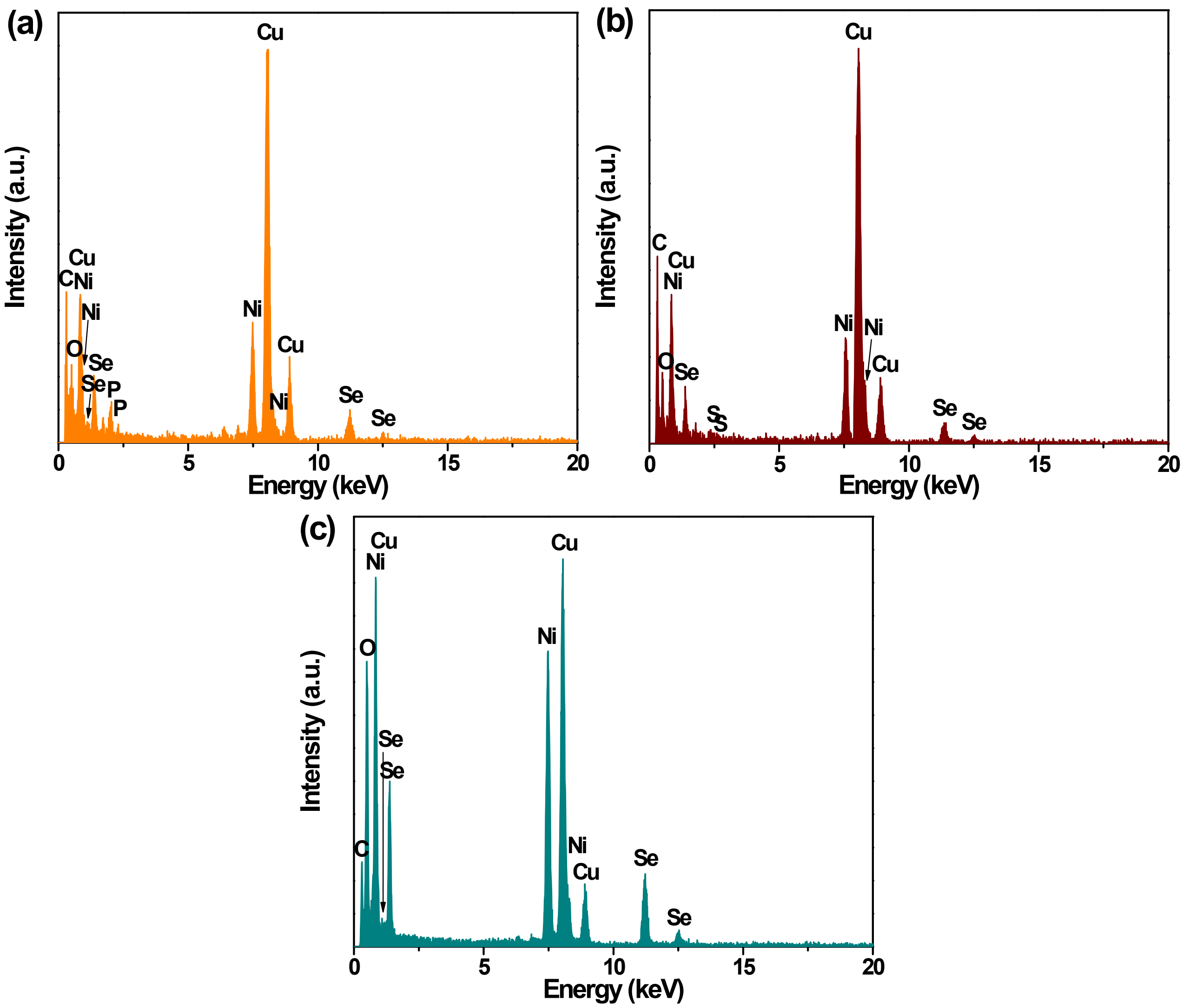

Figure S3. STEM-EDX spectra of the as-prepared (a) Ni_2P/Ni_3Se_4-5.0, (b) Ni_3S_4/Ni_3Se_4-5.0, and (c) $NiSe_2/Ni_3Se_4$-5.0. The Cu, C, and O signals stem from the copper grid used for TEM imaging, carbon supporting film, and oxidized surface species of the samples, respectively.

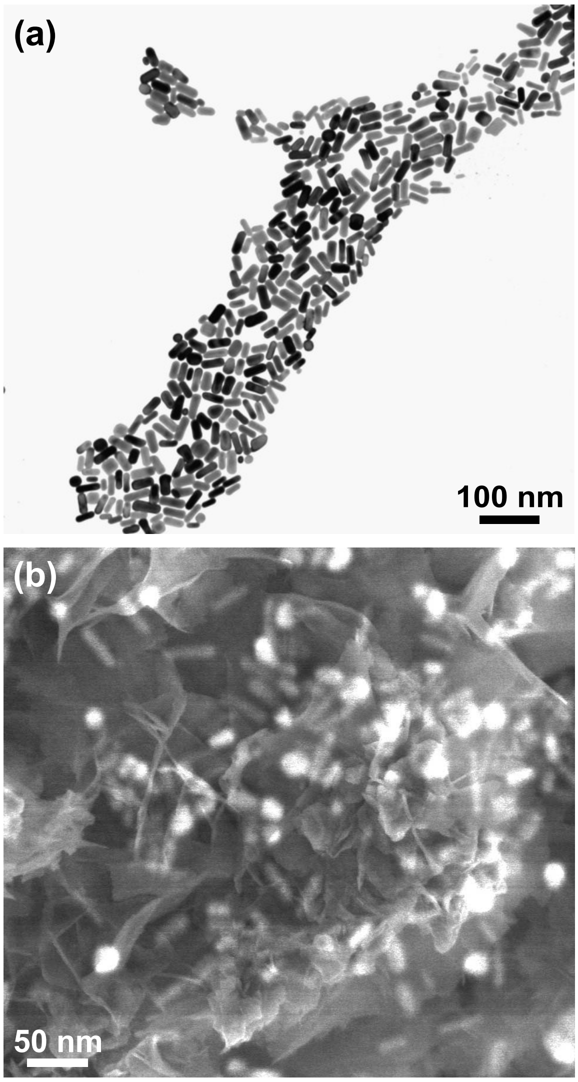

Figure S4. (a) TEM and (b) SEM images of the as-prepared (a) Ni_3S_4 NRs and (b) Ni_3S_4/Ni_3Se_4-5.0.

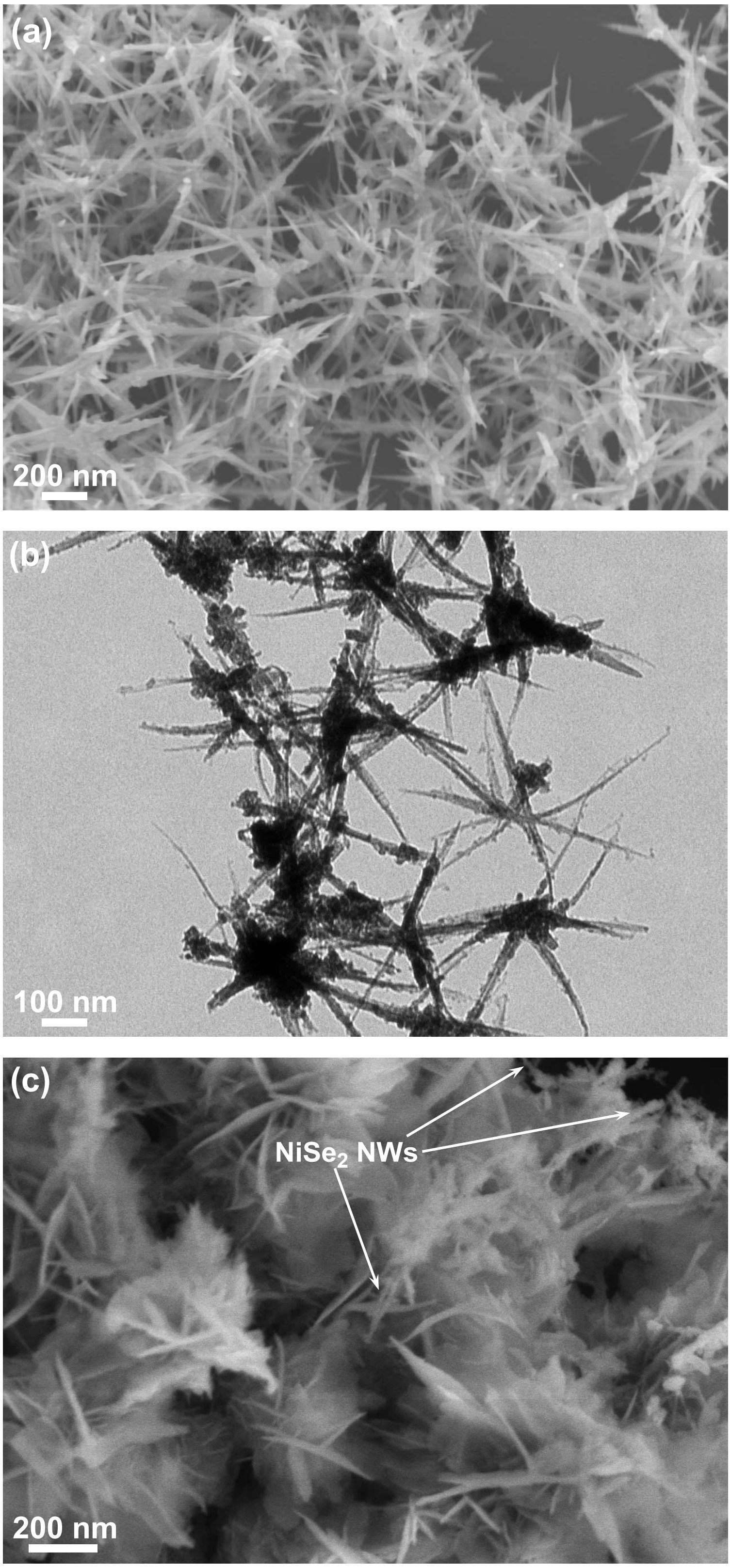

Figure S5. (a and c) SEM and (b) TEM images of the as-prepared (a and b) $NiSe_2$ NWs and (c) $NiSe_2/Ni_3Se_4$-5.0.

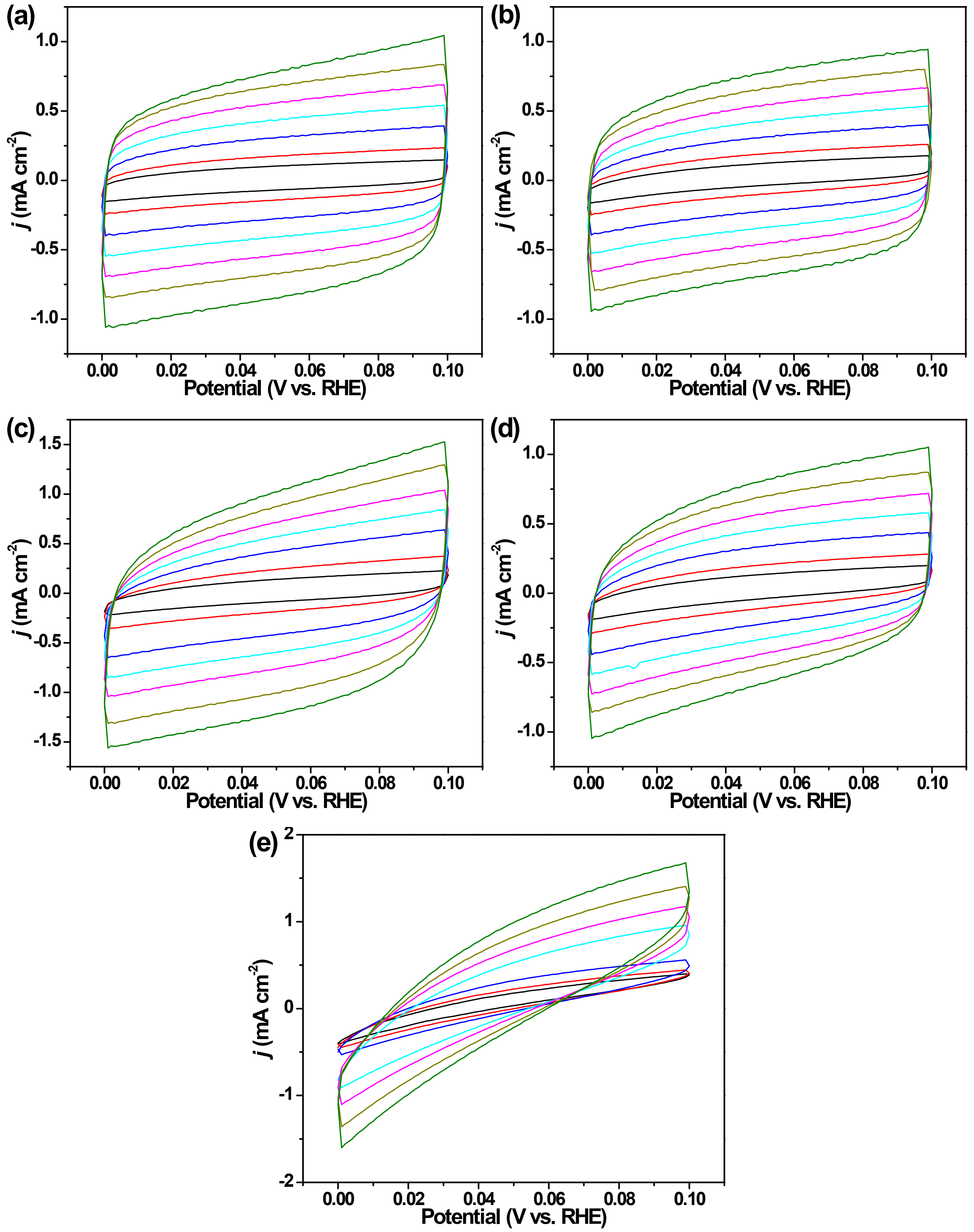

Figure S6. CV curves of (a) Ni_2P/Ni_3Se_4-2.5, (b) Ni_2P/Ni_3Se_4-5.0, (c) Ni_2P/Ni_3Se_4-7.5, (d) Ni_3Se_4 NSs/NF, and (e) Ni_2P NPs/NF electrodes recorded in 1 M KOH aqueous solution. Scan rates of 5, 10, 20, 30, 40, 50, and 60 mV s^{-1} were chosen.

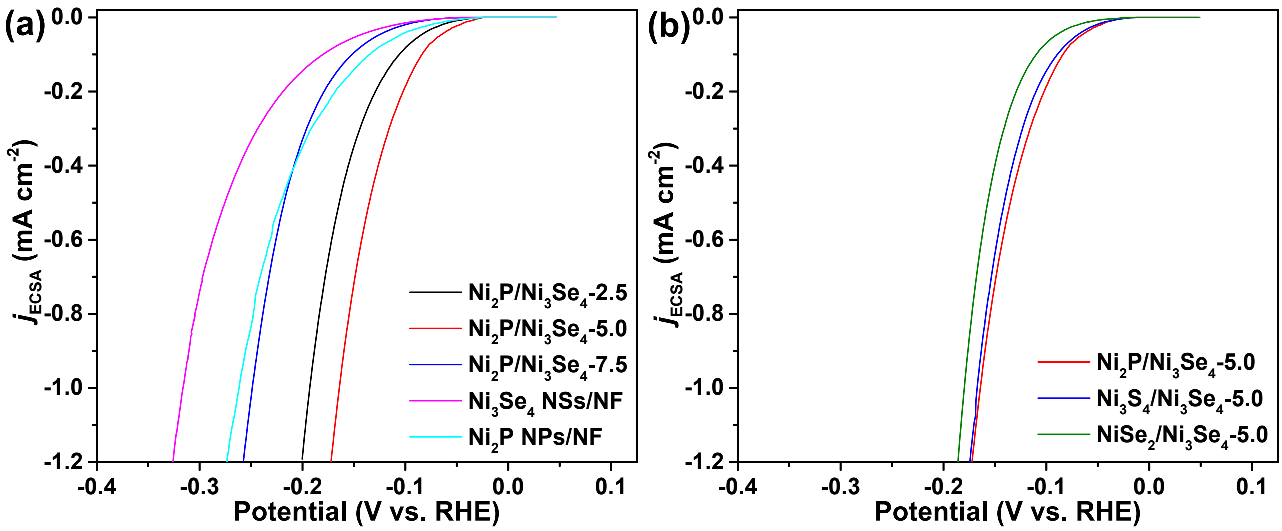

Figure S7. (a and b) Normalized polarization curves of various electrocatalysts measured in 1 M KOH, where the j of each electrocatalyst is normalized to the ECSA of the corresponding electrocatalyst. A specific capacitance of 0.040 mF cm^{-2} is adopted in 1 M KOH.

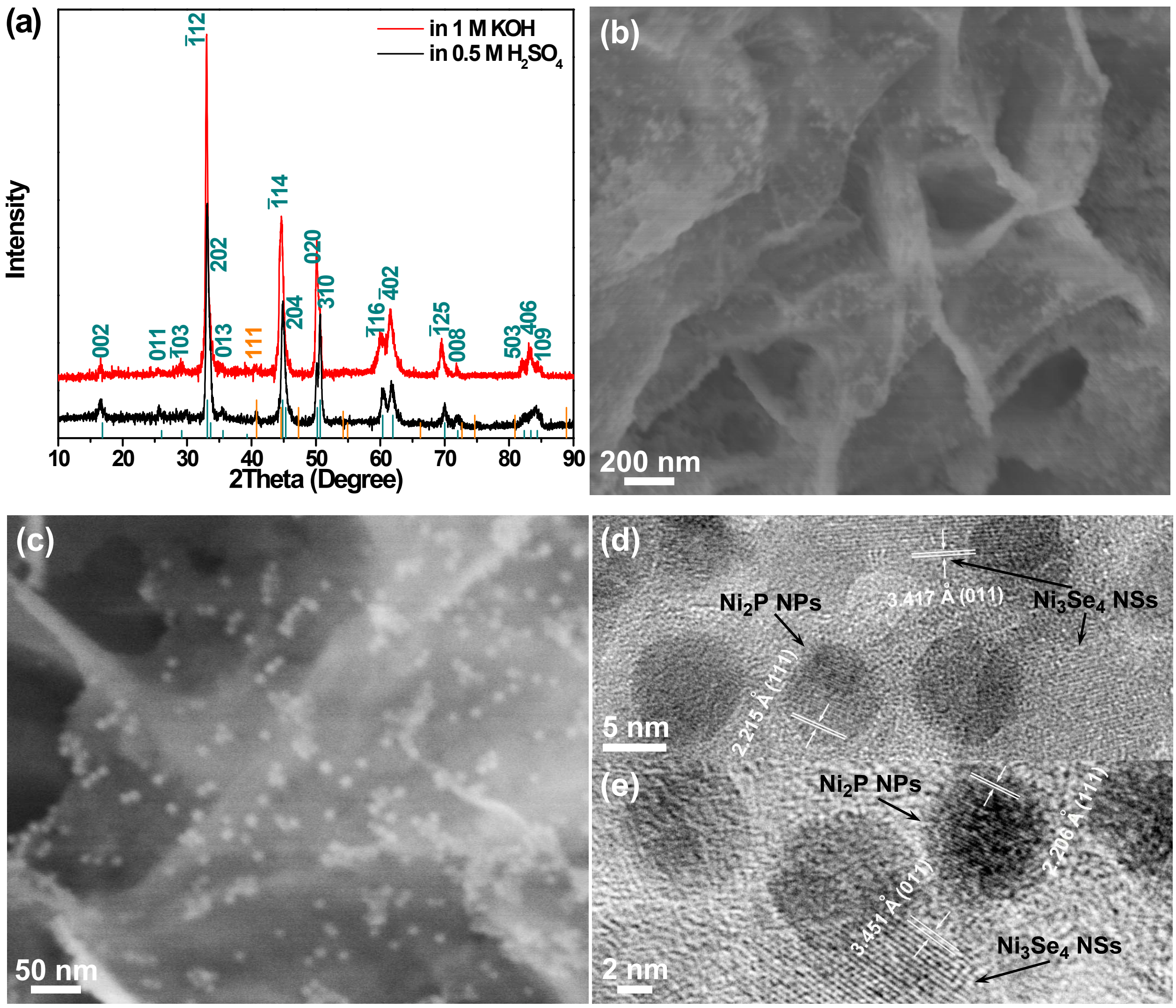

Figure S8. (a) XRD patterns, (b and c) SEM, and (d and e) HRTEM images of the Ni_2P/Ni_3Se_4-5.0 obtained after

CP measurement at a j of 20 mA cm^{-2} for the HER over a period of 50 h in (b and d) 1 M KOH and (c and e) 0.5 M H_2SO_4.

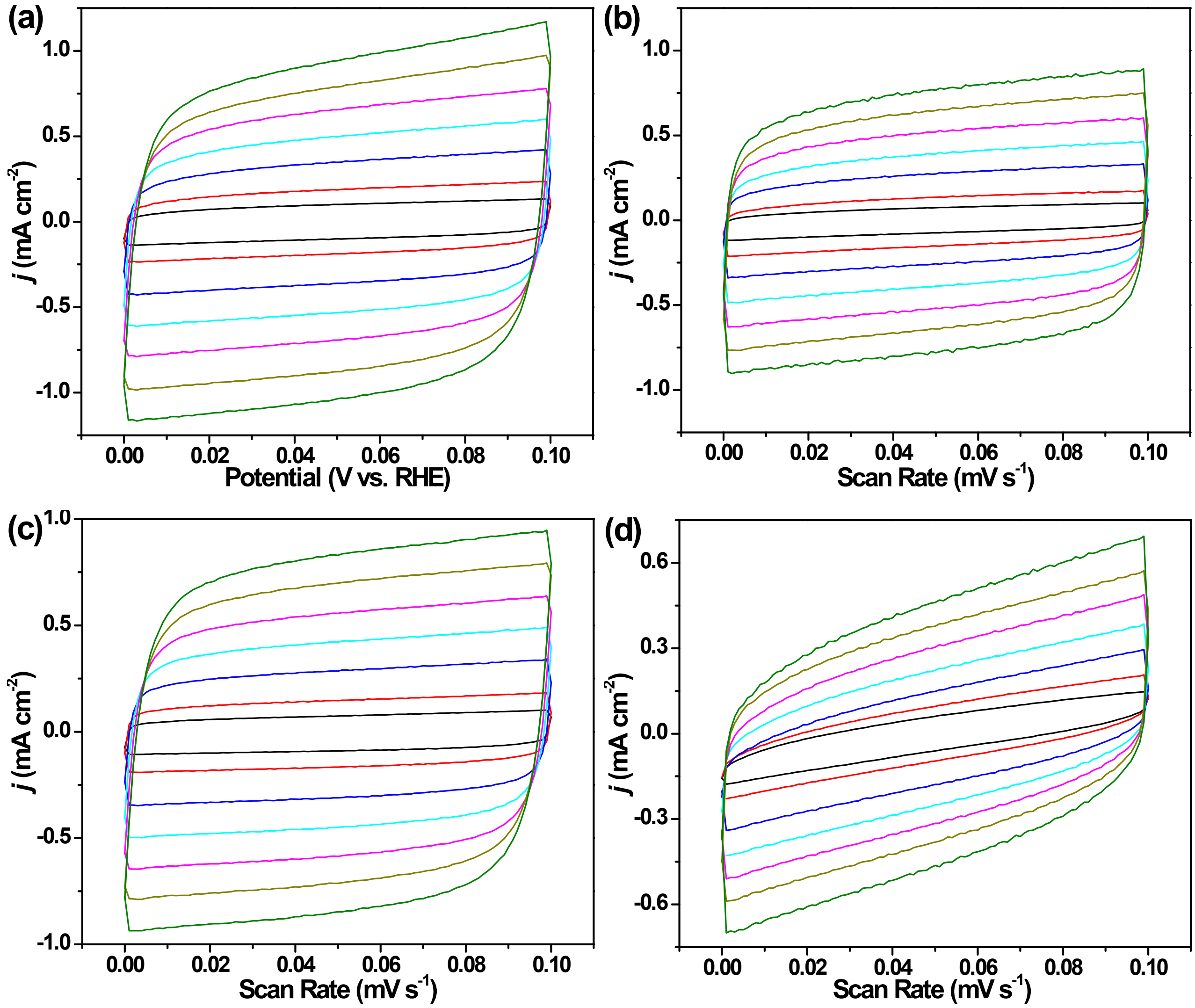

Figure S9. CV curves of (a) Ni_3S_4/Ni_3Se_4-5.0, (b) Ni_3S_4 NRs/NF, (c) $NiSe_2/Ni_3Se_4$-5.0, and (d) $NiSe_2$ NWs/NF electrodes obtained in 1 M KOH aqueous solution. Scan rates of 5, 10, 20, 30, 40, 50, and 60 mV s^{-1} were chosen.

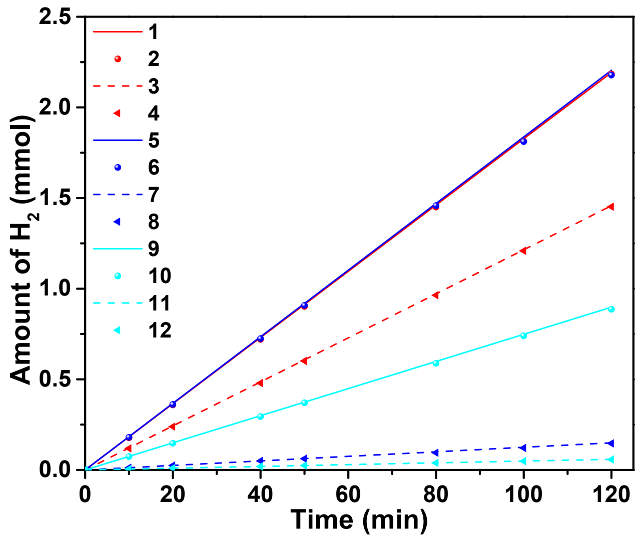

Figure S10. The time evolution of the measured amount of the produced H_2 (plots 2, 4, 6, 8, 10, and 12) with respect to the theoretically calculated values assuming a 100% Faradaic efficiency for the HER (plots 1, 3, 5, 7, 9, and 11). Plots 1−4, 5−8, and 9−12 are recorded from the Ni_2P/Ni_3Se_4-5.0, Ni_3S_4/Ni_3Se_4-5.0, and $NiSe_2/Ni_3Se_4$-5.0, respectively, in 1 M KOH (plots 1, 2, 5, 6, 9, and 10) or 0.5 M H_2SO_4 (plots 3, 4, 7, 8, 11, and 12). All the values are obtained at an η of 0.1 V.

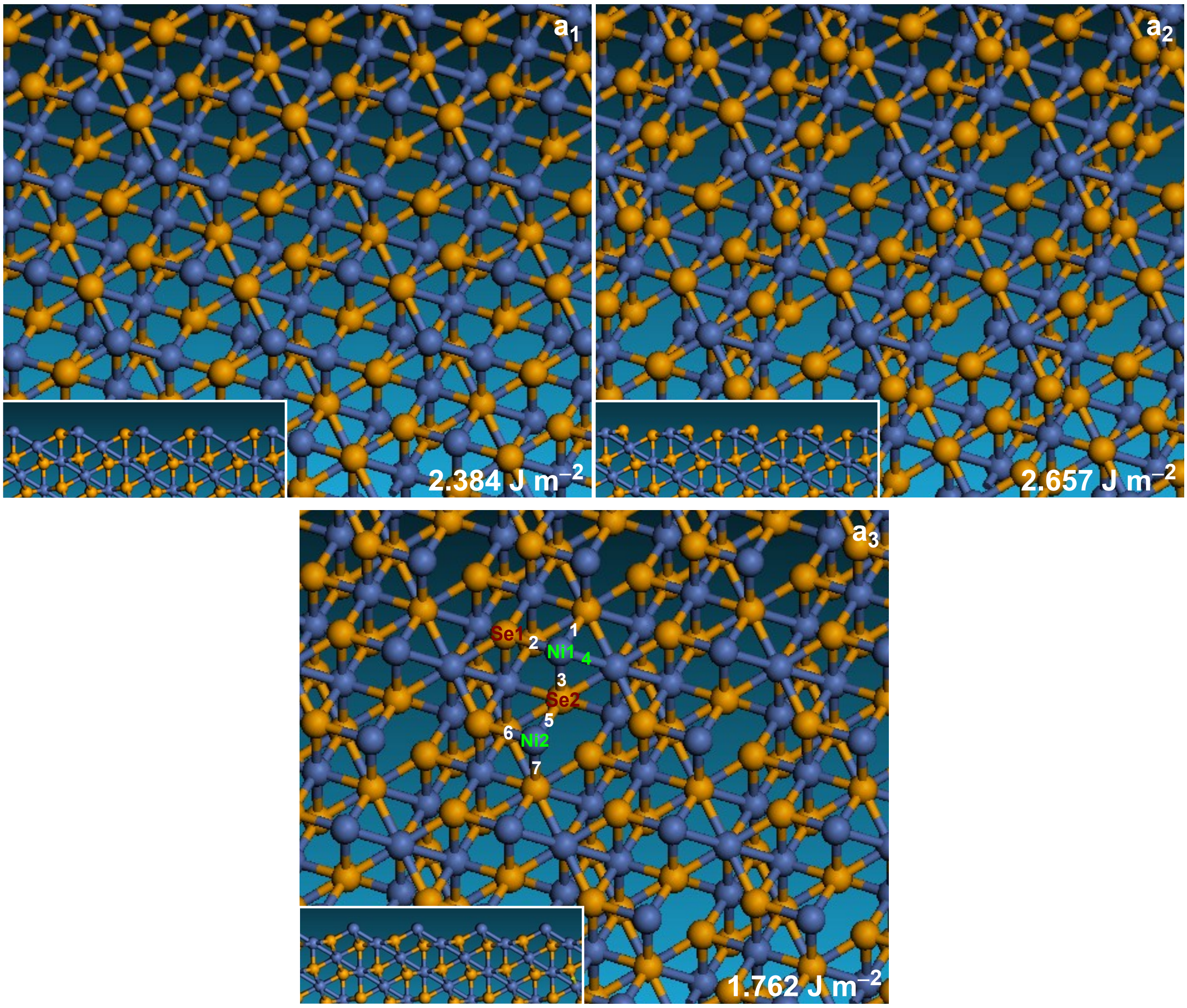

Figure S11. Top and side view (insets) models of possible exposed terminations for the (−112) surface structure of Ni_3Se_4, showing three types of (−112) facets with different terminations. The blue and yellow balls represent Ni and Se atoms, respectively. The surface energy is computed to be 2.384, 2.657, and 1.762 J m^{-2} for a_1, a_2, and a_3, respectively.

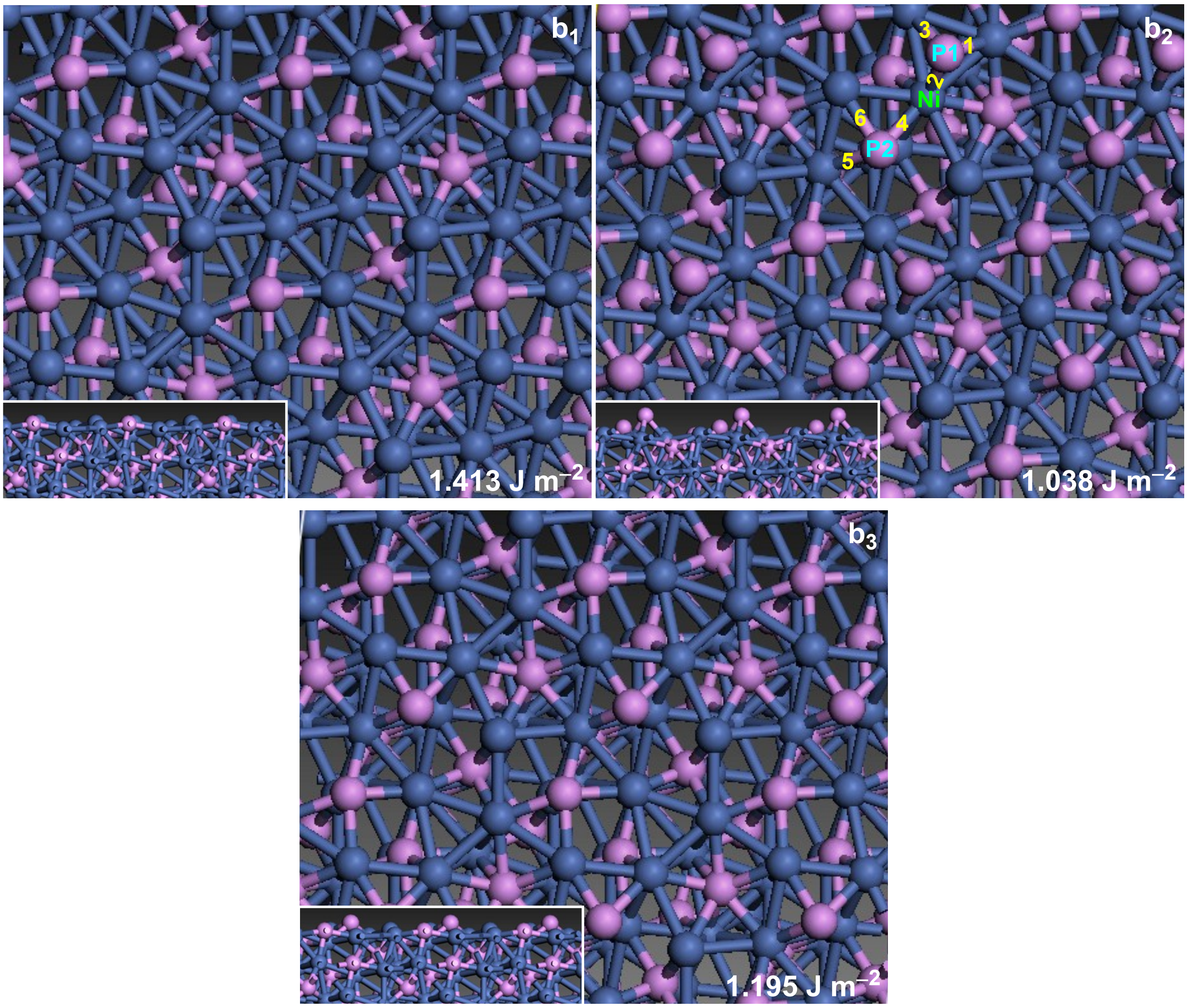

Figure S12. Top and side view (insets) models of possible exposed terminations for the (111) surface structure of Ni_2P, showing three types of (111) facets with different terminations. The blue and pink balls represent Ni and P atoms, respectively. The surface energy is computed to be 1.413, 1.038, and 1.195 J m^{-2} for b_1, b_2, and b_3, respectively.

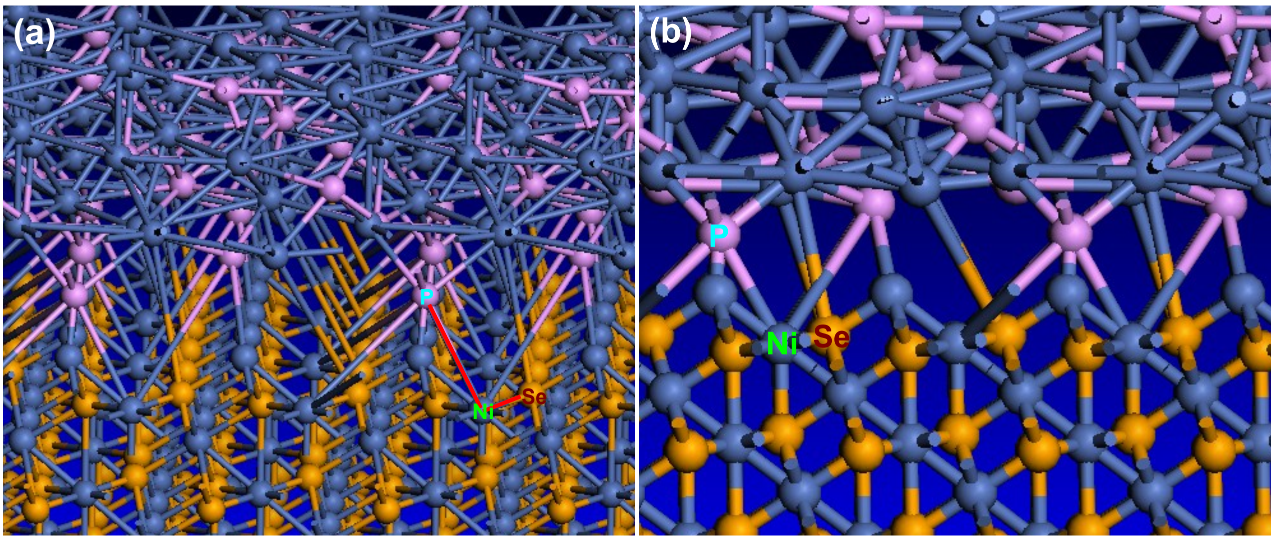

Figure S13. (a) Oblique and (b) side view models of the interface structure of $Ni_2P(111)/Ni_3Se_4(-112)$. The labeled Se and P atoms are the most likely active sites for the HER due to the interfacial P−Ni−Se bond (marked by the red lines).

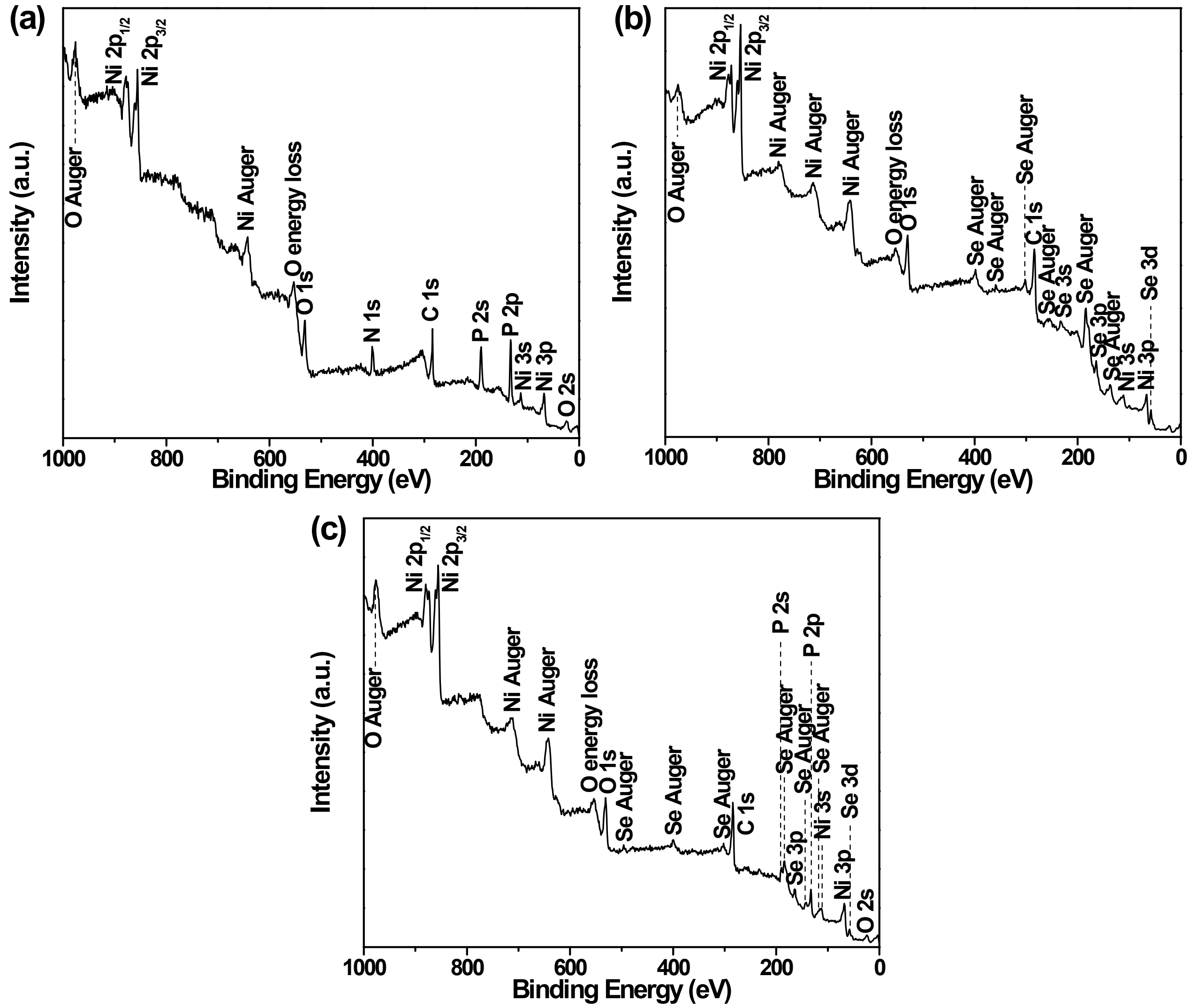

Figure S14. XPS survey spectra collected from (a) the Ni_2P NPs, (b) Ni_3Se_4 NSs, and (c) Ni_2P/Ni_3Se_4-5.0. The O peaks are attributed to the inevitable surface oxides.

Table S1. Comparison of the electrocatalytic activity of the previously reported Ni_2P and Ni_3Se_4 catalysts in the literature with X/Ni_3Se_4-5.0 in this work for the HER

catalyst/electrode	η (mV) at j (mA cm^{-2})	Tafel slope (mV dec^{-1})	loading (mg cm^{-2})	electrolyte	Ref
Ni_2P NPs/Ti	−180 at −100	−81	~1	0.5 M H_2SO_4	29
Ni_2P NPs/GCE	−250 at −20	−100	0.38	1 M KOH	30
	−140 at −20	−87		1 M H_2SO_4	
Ni_2P NPs/GCE	−137 at −10	−49	1.99	0.5 M H_2SO_4	31
Ni_2P/NF	ca. −150 at −10	−93	not mentioned	1 M KOH	34
Ni_2P hollow microspheres/GCE	−98 at −10	−86.4	0.283	1 M KOH	35
Ni_3Se_4 nanoassemblies/Ni	−208 at −50	−156	2.4	1 M KOH	36
Ni_2P/NF	−99 at −10 −126 at −20 −208 at −100	−96	5	1 M KOH	in this work
	−100 at −10 −126 at −20 −205 at −100	−93	5	0.5 M H_2SO_4	
Ni_3Se_4 NSs/NF	−206 at −50	−113	1.6	1 M KOH	in this work
	−209 at −50	−96	1.6	0.5 M H_2SO_4	

Table S2. Comparison of the electrocatalytic activity of various hybrid h-NMs catalysts in the literature with the X/Ni_3Se_4-5.0 in this work for the HER

catalyst/electrode	η (mV) at j (mA cm^{-2})	Tafel slope (mV dec^{-1})	loading (mg cm^{-2})	electrolyte	Ref in the text
Ni/NiO/$CoSe_2$/GCE	ca. −80 at −10 < −200 at −100	−39	0.28	0.5 M H_2SO_4	6
MoS_2/$CoSe_2$/GCE	−68 at −10	−36	0.28	0.5 M H_2SO_4	7
Co_9S_8@MoS_2/CNFs	−190 at −10	−110	0.212	0.5 M H_2SO_4	8
EG/$Co_{0.85}$Se/NiFe-LDH	−260 at −10	−160	4	1 M KOH	9
NiFe/$NiCo_2O_4$/NF	−105 at −10	−88	0.15	1 M KOH	10
MoO_x/Ni_3S_2/NF	−106 at −10 −224 at −100	−90	> 12	1 M KOH	11
MoS_2/Ni_3S_2/NF	−110 at −10	−83	9.7	1 M KOH	12
MoS_2−Ni_3S_2 HNRs/NF	−98 at −10 −191 at −100	−61	13	1 M KOH	13
$Ni_xCo_{3-x}S_4$/Ni_3S_2/NF	−136 at −10 −258 at −100	−107	0.56	1 M KOH	14
EG/Ni_3Se_2/Co_9S_8/graphite	ca. −150 at −10 −230 at −50	−83	2.5	1 M KOH	15
MoS_2/NiCo-LDH/NF	−78 at −10 −170 at −100	−77	3.5−4.0	1 M KOH	16
CoS_2@WS_2/CC	−97 at −10	−66	CoS_2: 2.0 WS_2: 1.0	0.5 M H_2SO_4	17
Co_9S_8/WS_2 nanobelt/Ti	−138 at −10	−80	2.2	1 M KOH	18
Co_3S_4@MoS_2/GCE	−210 at −10	−88	0.283	0.5 M H_2SO_4	19
TiO_2 NDs/Co NSNTs-CFs	−108 at −10 −235 at −100	−62	0.75	1 M KOH	20
Cu NDs/Ni_3S_2 NTs-CFs	−128 at −10	−76.2	0.52	1 M KOH	21
MoS_2/$NiCo_2S_4$/CFP	−140 at −10 −173 at −100	−38	not mentioned	0.5 M H_2SO_4	22
CeO_2–Cu_3P/NF	−91 at −15	−132	not mentioned	1 M KOH	23
MoS_2/Co_3S_4/GCE	−175 at −10 −220 at −100	−56 −115	0.285	0.5 M H_2SO_4 1 M KOH	24
CoP_3/Ni_2P/GCE	−115 at −10	−49	0.31	0.5 M H_2SO_4	25
MoS_2/NiS NCs/NF	−92 at −10	−113	4.9	1 M KOH	26
FeS_2/CoS_2 NSs/NF	−78 at −10	−44	0.2	1 M KOH	27
Co_3S_4/MoS_2/Ni_2P/GCE	−178 at −10	−98	0.144	1 M KOH	28
NiS–MoS_2 HNSAs/CC	−106 at −10	−57	2.8	1 M KOH	29
MoS_2/NiS_2 nanosheets/CC	−62 at −10 −131 at −100	−50	1.1	1 M KOH	30
Co_9S_8-MoS_2@3DC	−177 at −10 −230 at −10	−84 −112	1.0	1 M KOH 0.5 M H_2SO_4	31
$CoSe_2$@$MoSe_2$/GCE $CoSe_2$@$MoSe_2$/NF	−183 at −10 −183 at −10	−43 −88	0.53 0.60	0.5 M H_2SO_4 1 M KOH	32
Ni_2P–NiP_2 HNPs/NF	−60 at −10	−59	5	1 M KOH	33
NiSe-$Ni_{0.85}$Se/CP	−101 at −10	−74	1.68	1 M KOH	34
TiO_2@ Ni_3S_2	−112 at −10 −170 at −100	−69	not mentioned	1 M KOH	35
NiFe LDH@Ni_3S_2/NF	−184 at −10	−115	not mentioned	1 M KOH	36
Ni_2P/Ni/NF	−98 at −10	−72	not mentioned	1 M KOH	46
NF@Ni_2P/C NF@Fe_2−Ni_2P/C	ca. −85 at −10 −39 at −10	−57 −30	not mentioned 3.9 ± 0.3	1 M KOH	49
Ni_2P/Ni_3Se_4-5.0/NF	−57 at −10 −118 at −100 −76 at −10 −122 at −100	−54 −40	Ni_2P: 5.0 Ni_3Se_4: 1.6	1 M KOH 0.5 M H_2SO_4	in this work
Ni_3S_4/Ni_3Se_4-5.0/NF	−55 at −10 −116 at −100	−46	Ni_3S_4: 5.0 Ni_3Se_4: 1.6	1 M KOH	in this work

	−113 at −10 −156 at −100	−36		0.5 M H_2SO_4	
$NiSe_2/Ni_3Se_4$-5.0/NF	−78 at −10 −140 at −100	−56	$NiSe_2$: 5.0 Ni_3Se_4: 1.6	1 M KOH	in this work
	−132 at −10 −176 at −100	−42		0.5 M H_2SO_4	

Table S3. Lattice parameters (Å) of supercells for various model catalysts

catalyst	*a*	*b*	*c*
Ni_3Se_4	6.351	7.202	21.970
Ni_2P	6.760	6.760	21.589
$Ni_2P(111)/Ni_3Se_4(-112)$	6.555	6.981	21.891

Table S4. Comparison of the DFT computations for the H* at different surface adsorption sites on the (−112) surface (a_3) of Ni_3Se_4 and (111) surface (b_2) of Ni_2P.

adsorption site on a_3	ΔE_{H*} (eV)	ΔZPE (eV)	ΔG_{H*} (eV)	adsorption site on b_2	ΔE_{H*} (eV)	ΔZPE (eV)	ΔG_{H*} (eV)
Ni1	−0.908	0.027	−0.681	P1	0.019	0.028	0.247
1	−0.862	0.035	−0.627	1	0.196	0.034	0.430
2	−0.771	0.035	−0.536	3	0.190	0.033	0.423
4	−0.830	−0.074	−0.704	P2	0.026	0.030	0.256
Se1	−0.667	0.031	−0.436	4	0.188	0.031	0.419
Ni2	−1.035	0.027	−0.808	6	0.178	0.033	0.411
5	−0.921	0.032	−0.689	Ni	−0.797	0.032	−0.565
7	−0.928	0.033	−0.695				
Se2	−0.626	0.032	−0.394				